Received February 26, 2020, accepted March 18, 2020, date of publication April 20, 2020, date of current version May 8, 2020.

Digital Object Identifier 10.1109/ACCESS.2020.2988881

Novel Interference Suppression Null Steering Antenna System for High Precision Positioning

ARPAN PAL[1], (Member, IEEE), AMIT MEHTA[1], (Senior Member, IEEE), ANDREW SKIPPINS[1], PAUL SPICER[1], AND DARIUSH MIRSHEKAR-SYAHKAL[2], (Fellow, IEEE)

[1]College of Engineering, Swansea University, Swansea SA2 8PP, U.K.
[2]Department of Computing Science and Electronic Engineering, Essex University, Colchester CO4 3SQ, U.K.

Corresponding authors: Arpan Pal (pal.arpan@gmail.com) and Amit Mehta (a.mehta@swansea.ac.uk)

This work was supported in part by the MBDA, U.K., and MBDA, France.

ABSTRACT The high precision (centimetre accuracy) positioning systems are set to play a key role in revolutionising smart farming, self-driving cars, drone deliveries, heavy machine navigation, etc. With so much at stake the technology also needs protection from an intentional sabotage or denial of service. It is very easy with current satellite-based navigation jammers to disrupt a navigation service. Our proposed technology solves this challenge in a compact and cost-effective way. Compared to normal navigation patch antennas our proposed dual ring antenna offers over 30 dB of protection. Thus, if a patch antenna-based navigation system is disturbed at 1 watt of interference power, it will take 1000 watts to disrupt navigation system working on our proposed system. With the size of only 130 mm × 130 mm and cheap large-scale manufacturing, our proposed antenna is perfectly suitable for applications for safety and prosperity of the smart nation-based living.

INDEX TERMS Jamming, null steering, capacitive coupling, adaptive algorithm, raspberry Pi.

I. INTRODUCTION

High precision positioning can be achieved by combining multiple GNSS (Global Navigation Satellite Systems) for UAVs (Unmanned Arial Vehicles), automated and connected agriculture, interconnected cars and robotic guidance. This precision can easily be sabotaged by a cheap off the shelf 1.5 GHz GNSS jammer, which would disturb the acquisition and tracking of navigation satellites and lead to incorrect position, velocity, or time information as shown in the Fig. 1. The jamming (or interference) cancellation systems which currently are on market [1] consist of at least three or more antennas working in tandem, are of a very large in size (300 mm × 300 mm) and are expensive. Both of these attributes will rule them out for small platform implementation in the above-mentioned applications. We propose a new type of single antenna solution which is much smaller in size (130 mm × 130 mm) and much lower in final large-scale price.

Several configurations of single element null steering antennas were investigated over the past few years. PIN [2] and Varactor [3] diodes are used in slot antennas for achieving discrete null steering operation. Multiple modes for pattern reconfigurable antennas [4]–[9] are exploited for achieving continuous null steering functionality.

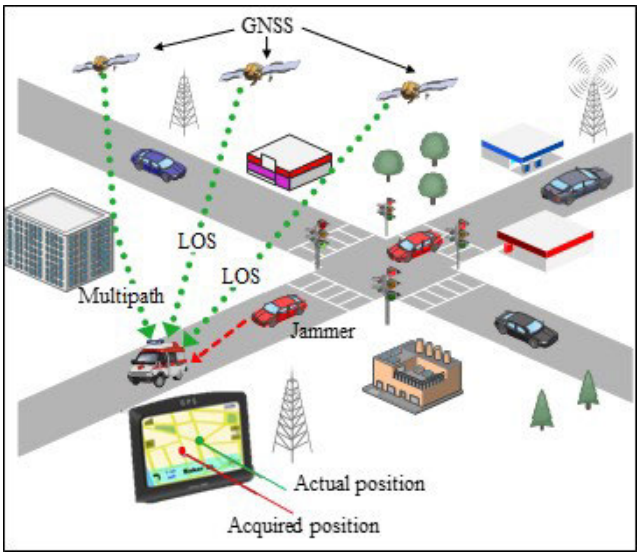

FIGURE 1. Jamming/Interference could lead the navigation system to 'out of operation' and could provide wrong information of the real position.

The associate editor coordinating the review of this manuscript and approving it for publication was Giovanni Angiulli.

This work is licensed under a Creative Commons Attribution 4.0 License. For more information, see https://creativecommons.org/licenses/by/4.0/

Indeed, Jiang *et al.* [4] combined radiation from even and odd modes in a shorted patch antenna to achieve two dimensional (2D) null scanning. Li *et al.* [5] combined radiation patterns from a vertical monopole and a patch antenna for a pseudo three dimensional (3D) continuous null steering. Soloman [6] employs multiple ports in a rectangular patch antenna to excite circularly polarized axial beam and linearly polarized conical beam simultaneously.

The combination of these beams provides a circularly polarized main beam and a steerable null in the lower elevation angles. Deng *et al.* [7] achieved a 3D continuous null steering by combining circularly polarized axial mode of a truncated patch antenna and circularly polarized conical beam mode of four rotationally symmetric strips. In further works [8]–[10], multiple radiating modes of concentric shorted patch antennas are investigated for providing full hemispherical null steering. However, in that design the use of shorting metal pins results in a complex, costly and heavy antenna structure, low fabrication repeatability, machining requirement in the manufacturing which all lead to high final product price. In this paper, a Slot Based Microstrip Patch Antenna (SBMPA) is investigated for providing null steering in the entire upper hemisphere. The proposed antenna has a circular patch with multiple slots nested inside a concentric circular ring patch. The antenna has no shorting pins and therefore does not suffer from the previously mentioned drawbacks of complexity, weight and cost. We also present our fully developed and deployed system for demonstrating the autonomous null steering capabilities. Table 1 provides a comparison of this work with those of similar works [3], [4], [7]–[8]. It shows the significant contributions of this work in achieving a system with low-profile compact light weight structure, and of excellent null depths. For the first time this paper presents the integration with the GNSS receiver and an autonomous null steering mechanism.

TABLE 1. Performance comparison between the proposed antenna and antennas reported in [3], [4], [7] and [8] (λ_0 is the free space wavelength at the operating frequency).

	This work	[3]	[4]	[7]	[8]
Operating frequency (GHz)	1.575	2.4	2.4	1.575	1.575
Height	$\lambda_0/60.7$	$\lambda_0/39.4$	$\lambda_0/21$	$\lambda_0/14.7$	$\lambda_0/59.5$
Size	$0.68\lambda_0 \times 0.68\lambda_0$	$1.23\lambda_0 \times 1.23\lambda_0$	$0.96\lambda_0 \times 0.8\lambda_0$	$0.47\lambda_0 \times 0.47\lambda_0$	$1.05\lambda_0 \times 1.05\lambda_0$
Bandwidth (MHz)	26	50	80	87	22
Polarization	CP	LP	LP	CP	CP
Max Null depth (dB)	45	47	45	26	40
Design aspects	Planar lighter structure	Varactors required	Slots in GND	Air gap between 2 layers	32 vias
Feeding network	Yes	No	No	No	Yes
Integration with GNSS receiver	Yes	No	No	No	No
Autonomous null steering mechanism	Yes	No	No	No	No
Field trails: performance validation	Yes	No	No	No	No

II. NULL STEERING ANTENNA SYSTEM

Fig. 2 shows the complete configuration of the implemented null steering antenna system. It consists of three sections: SBMPA, feed network and receiver. The SBMPA consists of an inner circular patch and the outer circular ring and provides RHCP axial beam and conical beam, respectively. The feeding network is designed to combine these two radiation beams with different phase and amplitude ratio. It is composed of power divider/combiners, Low noise Amplifier (LNA) [11], Phase Shifters (PS) [12] and Variable Gain Amplifier (VGA) [13]. The two ports P_1 and P_2 of the inner patch are connected to the two input ports of a 2:1 power combiner/divider (PC1) using two flexible coaxial cables each having a length of 100 mm. Delay lines are used in the power combiner to provide the 90° phase difference between the two signal paths. The output of the power combiner is connected to a Low Noise Amplifier (LNA) whose output is further connected to a 4-bit digital PS. Similarly, two ports P_3 and P_4 are connected to a VGA using PC2 and an LNA. Both the outputs of the PS and VGA are connected to a NovAtel FlexPak6 GNSS receiver [14] using a 2:1 power combiner (PC3). The biasing and controlling voltages for the PS and VGA are provided using a Raspberry Pi3. A Graphical User Interface (GUI) is designed using Python programming language to electronically control phase shift and amplification states of the PS and VGA. The user can access the GUI using a display screen connected to the Pi. Raspberry Pi also runs a 'Scan, Monitor and Lock algorithm' for intelligently steering the null in the direction of arrival of interference.

A. SLOT BASED MICROSTRIP PATCH ANTENNA (SBMPA)

Fig. 3 shows the top, side and bottom views of the SBMPA. The antenna consists of a circular inner patch nested within a concentric outer circular ring patch. The antenna is designed on top of a Rogers RT5880B substrate (with $\varepsilon_r = 2.2$ and $\tan\delta = 0.0009$) [15] having an area of 130 mm × 130 mm and a thickness of 3.14 mm. The whole antenna structure is backed by a ground plane having a diameter of $l = 130$ mm. The inner patch with two feed points P_1 and P_2 is designed to excite TM_{11} mode [9] for providing a circularly polarized axial beam. The feed ports P_1 and P_2 are orthogonal to each other and located at the same distance of 9.26 mm from the

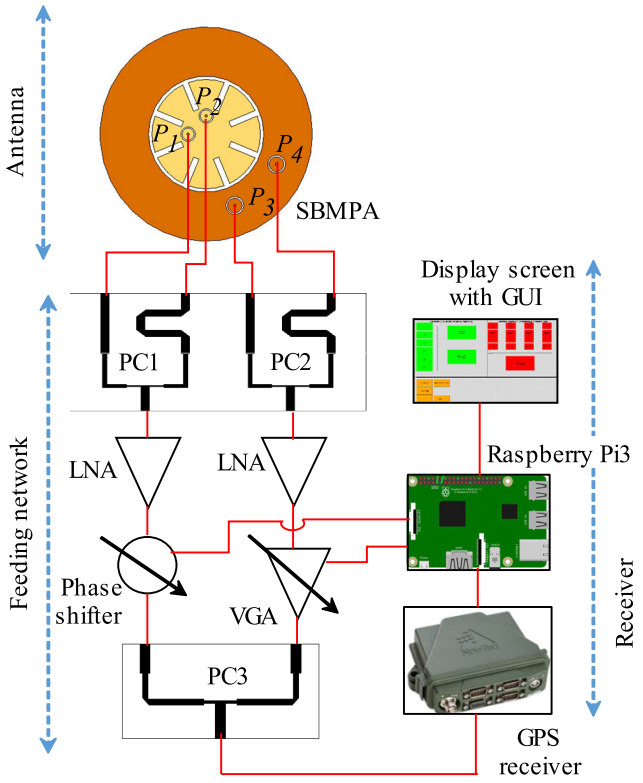

FIGURE 2. Complete configuration of the SBMPA based null steering system.

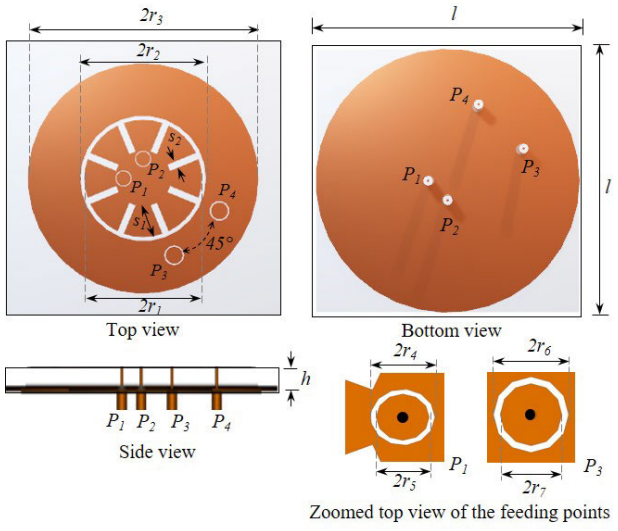

FIGURE 3. Top, side and bottom views of the SBMPA. l = 130 mm, h = 3.14 mm, $2r_1$ = 55.62 mm, $2r_2$ = 59.16 mm, $2r_3$ = 108.96 mm, $2r_4$ = 7.51 mm, $2r_5$ = 7.08 mm, $2r_6$ = 9.25 mm, $2r_7$ = 8.3 mm, S_1 = 14.62 mm and S_2 = 3 mm. The diameter for inner patch is referred to as $2r_1$ and for the outer patch is $2r_3$.

centre. Each feed point is connected to a vertical probe having a diameter of 1.3 mm and extending into the full thickness of the substrate. The probe is connected to a standard SMA (SubMiniature version A) connector attached at the ground plane. Eight rectangular slits are inserted into the circular patch. The slits increase the path length of the surface current as compared to that in the conventional circular patch, resulting in the reduction of the resonant frequency or reduction of the antenna size if the resonant frequency is to be maintained constant.

Fig. 4(a) shows the variation of the reflection coefficient at port P_1 with the slit length (S_1). The resonant frequency reduces by 20% (from 1.95 GHz to 1.575 GHz) if the slit length increases from 0 to 14.85 mm. In the proposed design of the antenna the slit length was selected to be 14.85 mm to obtain a resonant frequency of 1.575 GHz. The slit width was selected to be S_2 = 2 mm. The input impedance ($R_{in} + jX_{in}$) of the antenna designed for 1.575 GHz is found to be 269+j178 Ω when the inner patch is fed directly

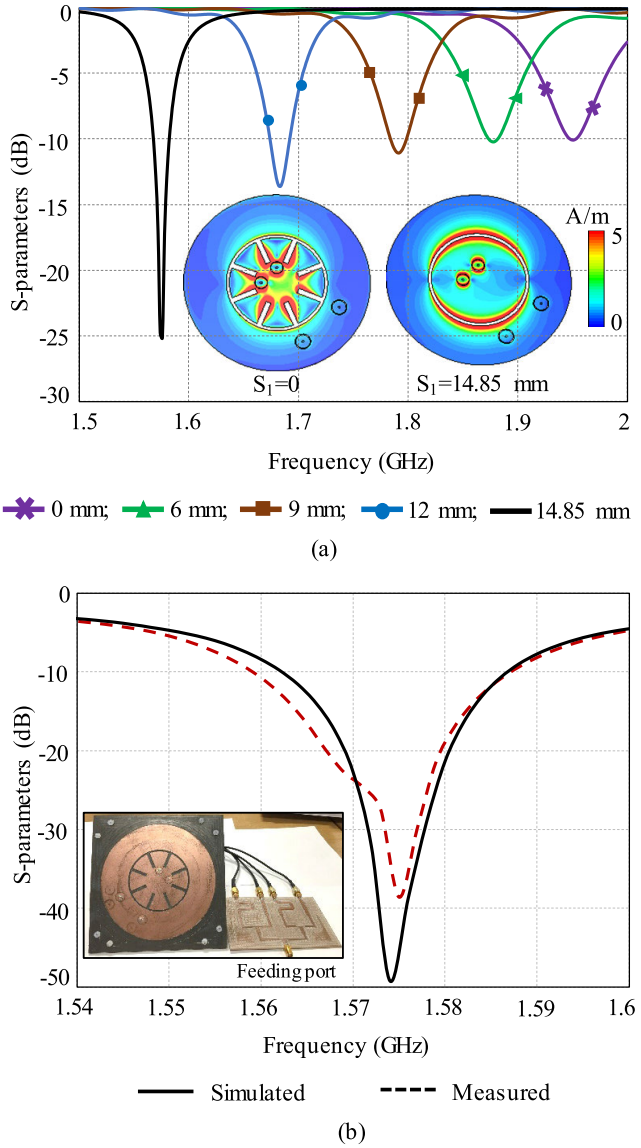

FIGURE 4. (a) Reflection coefficients ($|S_{11}|$) of the inner circular patch antenna for different slit length S_1. (b) Simulated and measured reflection coefficients of the SBMPA when all the four ports are excited simultaneously.

through the coaxial probe. This input impedance causes a large mismatch to the standard 50 Ω feedline and consequently, the gain and efficiency of the antenna reduce considerably. To tackle this problem a capacitively coupled feed system was developed. To this end, a circular slot having a width of 0.22 mm (r_4-r_5) is inserted around both feed points (P_1 and P_2) of the central patch. The circular coupling slot provides a series capacitance between the probe and the patch. This eliminates the high value of the inductance in the input impedance and transforms the large value of the resistance of the input impedance to an appropriate value. With this circular slot, the input impedance attains 49-j7 Ω enabling the antenna to achieve a good impedance match to the 50 Ω feed line at 1.575 GHz.

The outer annular ring patch is fed at two points P_3 and P_4 located at the same distance 39.2 mm from the centre. Similar to the inner patch, a circular capacitive coupling slots of width 0.48 mm (r_6-r_7) are inserted around its two outer feed points (P_3 and P_4) for achieving good impedance match to 50 Ω feed line. The two feed points P_3 and P_4 are separated by 45° along the circle passing through P_3 and P_4 points to excite TM_{21} conical beam modes [10]. We combined two radiation beams, one axial from the inner circular patch and one conical from the outer ring patch to create a null which can be steered in the space.

Fig. 4(b) shows the simulated and experimental reflection coefficients of the SBMPA when four ports are excited simultaneously using a 1:4 power divider (inset in Fig. 4(b)). The delay lines introduced in the power divider are for providing the quadrature excitation to both the inner patch and outer ring for achieving RHCP radiation. The ports of the SBMPA and power divider are connected using four 100 mm long co-axial cables each having a loss of 0.2 dB. The SBMPA covers the frequency band 1.562 GHz to 1.588 GHz meeting $|S_{11}| < -10$ dB criterion. The antenna provides a bandwidth of 26 MHz (1.65% with respect to centre frequency 1.575 GHz) which is narrow due to the extremely low profile (thickness $\approx \lambda_0/61$) of the antenna. However, it is sufficient for a single 20 MHz channel for GPS signal reception.

Fig. 5(a) shows the simulated and measured normalized radiation patterns of the TM_{11} mode of the inner circular patch and the TM_{21} mode outer ring patch antenna at 1.575 GHz. The inner patch has an RHCP axial beam when the two ports are excited simultaneously with signals of equal amplitude and phase difference of 90°. Fig. 5(a) (left column) shows 3D radiation pattern and polar cuts of the axial beam at $\phi = 0°$ and $\phi = 90°$ planes. The measured patterns are in good agreement with the simulated results. The gain for the axial beam is 7.6 dBi and the cross polarized discrimination (XPD) is greater than 25 dB in both the planes. It is observed that the axil beam covers the range of $-70° \leq \theta \leq 70°$ in the elevation plane with an axial ratio less than 3 dB. In contrast, an RHCP conical radiation pattern with a null in the broadside is obtained when the outer annular patch is excited simultaneously through its two ports with signals

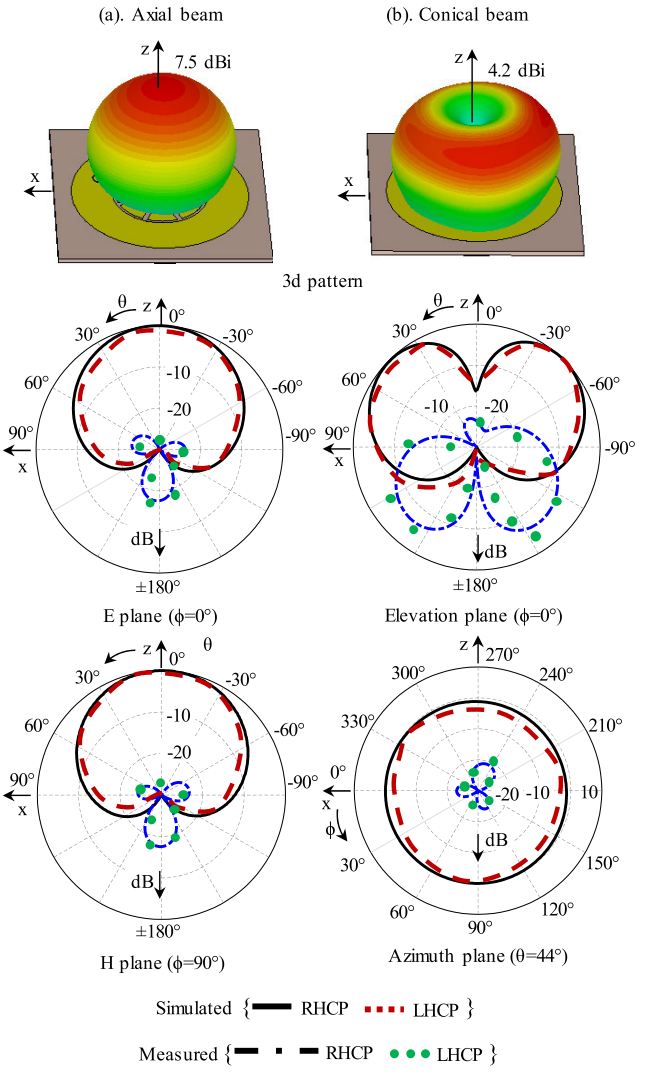

FIGURE 5. Radiation patterns of the inner patch and the outer ring at 1.575 GHz.

of equal amplitude and 90° phase difference at 1.575 GHz. Fig. 5(b) (right column) shows the 3D radiation patterns and polar cuts at elevation plane of $\phi = 0°$ and azimuth plane of $\theta = 44°$ of the conical beam due to TM_{21} mode. The beam achieves the maximum measured gain of 4.2 dBi in the direction of $\theta_{max} = \pm 44°$ and provides an omnidirectional coverage in the azimuth plane. The conical beam covers the range of $15° \leq \theta \leq 67°$ with an axial ratio of less than 3 dB in the elevation plane over all azimuth angels (ϕ).

B. FEEDING NETWORK

To demonstrate the null steering functionality of the SBMPA we developed the feeding network using low cost off-the-shelves components. The configuration of the feeding network is discussed in Section II. The null steering in both the elevation and the azimuth plane can be achieved by combining TM_{11} mode axial beam and TM_{21} mode conical beam with different amplitude ratio, α, and phase shift values, β,

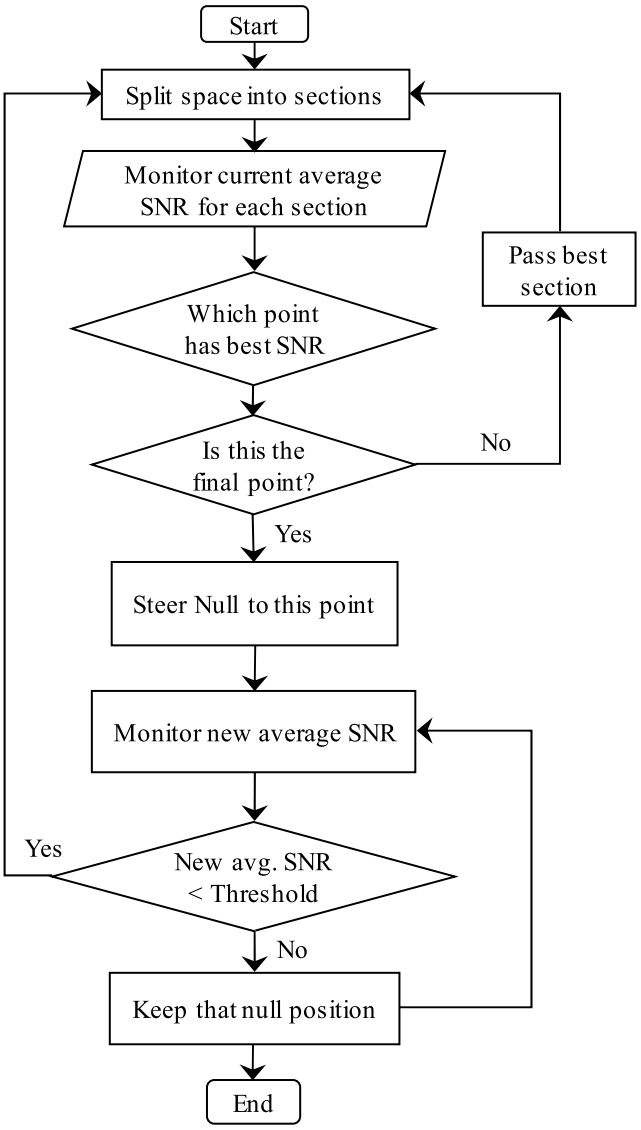

FIGURE 6. Null steering algorithm.

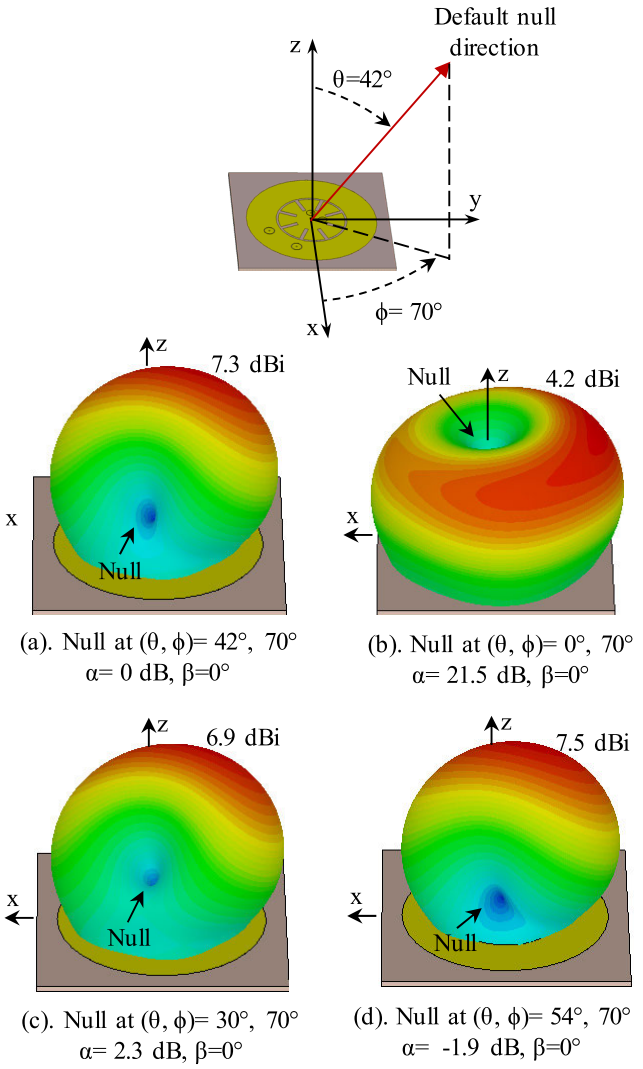

FIGURE 7. 3D radiation patterns of the SBMPA for different amplification factors at 1.575 GHz.

respectively. The α and β are given by

$$\alpha = \frac{|A_{p3}| + |A_{p4}|}{|A_{p1} + |A_{p2}|} \tag{1}$$

and

$$\beta = \angle\beta_{p1} - \angle\beta_{p3} = \angle\beta_{p2} - \angle\beta_{p4}$$

where, $|A_{p1}|$, $|A_{p2}|$, $|A_{p3}|$ and $|A_{p4}|$ are the amplitudes and $\angle\beta_{p1}$, $\angle\beta_{p2}$, $\angle\beta_{p3}$ and $\angle\beta_{p4}$ are the phases of the excitation signals at ports P_1, P_2, P_3 and P_4, respectively. As discussed earlier, the VGA and the phase shifter controls α and phase difference β, respectively.

C. RECEIVER

As discussed earlier in section II, the satellite signals are received using a NovAtel FlexPak6 GNSS receiver. An intelligent 'Scan, Monitor and Lock Algorithm (SMLA)' sits on the Raspberry pi and enables the SBMPA to automatically steer the beam null in the direction of the jamming/interference.

Fig. 6 shows the flow chart of the SMLA. SMLA monitors the SNR values of the all received satellite by accessing the NEMA-0183 [16] statements produced by the receiver. These statements contain several information of the received satellites such as PRN (Pseudo Random Number), total number of satellites received, SNR value of each satellite, elevation and azimuth angles, etc.

The SMLA upon initiating scans the null over entire hemispherical space in steps and monitors the average SNR values at each step. To reduce the scanning time both elevation and azimuth plane is split into four sections. The average SNR is monitored in the middle of each elevation section for each azimuth section. This method picks the best section with highest average SNR and discards the rest. Further, it splits the best section into four sections and look at the middle point.

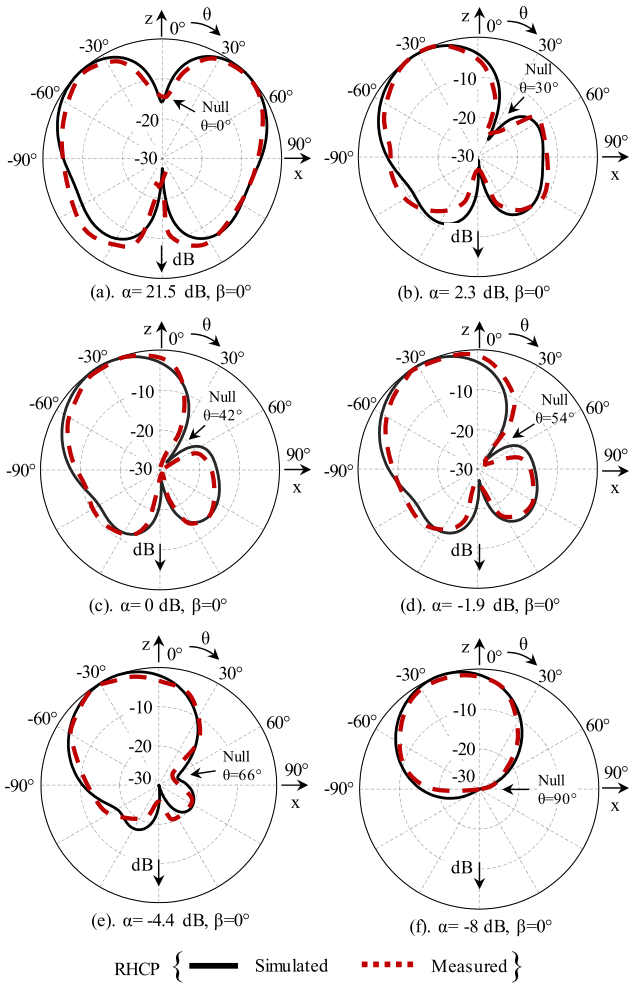

FIGURE 8. Null steering in the $\phi = 70°$ elevation plane at 1.575 GHz.

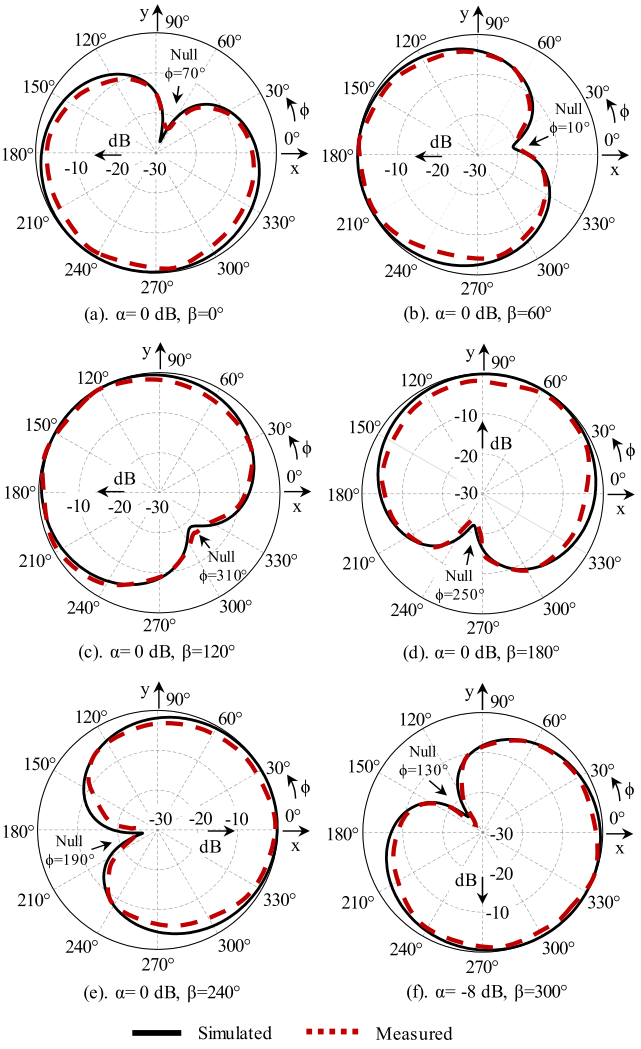

FIGURE 9. Null steering in the $\theta = 42°$ azimuth plane at 1.575 GHz.

The scan mechanism repeats automatically until only 4 points remain, finds the best SNR and lock the Null at this point.

III. NULL STEERING PERFORMANCE

The VGA provides 64 different amplitude states and the phase shifter provides 16 phase values. Therefore, there are a total of $64 \times 16 = 1024$ null configuration states which are available. Fig. 7 shows the 3D radiation pattern of the SBMPA for different values α with $\beta = 0°$. Fig. 7(a) shows the default null direction $(\theta, \phi) = 42°, 70°$ when all the four ports experience signals of equal amplitude in which case $\alpha = 0$ dB. The phase condition for the four ports are $\angle\beta_{p1} = \angle\beta_{p3} = 0°$ and $\angle\beta_{p2} = \angle\beta_{p4} = 90°$. This means phase difference between outer and inner ring $\beta = 0°$. A null depth of -45 dB at an angle of $\theta = +42°$ from the beam peak is observed in the default null direction. The direction of this null can be steered in elevation plane $\phi = 70°$ by changing the amplitude ratio α as shown in the Fig. 7 (a-d). The null moves toward the zenith ($\theta = 0°$) when the value of α increases, and towards the horizon ($\theta = 90°$) when α reduces. When the values of α are 21.5 dB, 2.3 dB and -1.9 dB,

TABLE 2. Null directions for different combination of α and β.

	α (dB)	β	Null direction	
			θ	ϕ
Fig. 8 (a)	21.5	0°	0°	70°
Fig. 8 (b)	2.3	0°	30°	70°
Fig. 8 (c)	0	0°	42°	70°
Fig. 8 (d)	-1.9	0°	54°	70°
Fig. 8 (e)	-4.4	0°	66°	70°
Fig. 8 (f)	-8	0°	90°	70°
Fig. 9 (a)	0	0°	42°	70°
Fig. 9 (b)	0	60°	42°	10°
Fig. 9 (c)	0	120°	42°	310°
Fig. 9 (d)	0	180°	42°	250°
Fig. 9 (e)	0	240°	42°	190°
Fig. 9 (f)	0	300°	42°	130°

the SBMPA provides a null in the direction of $\theta = 0°$, 30° and 54°, respectively in the $\phi = 70°$ plane. The null depth for these directions ($\theta = 0°$, 30° and 54°) are of -17.2 dB, -30.4 dB and -24.5 dB, respectively.

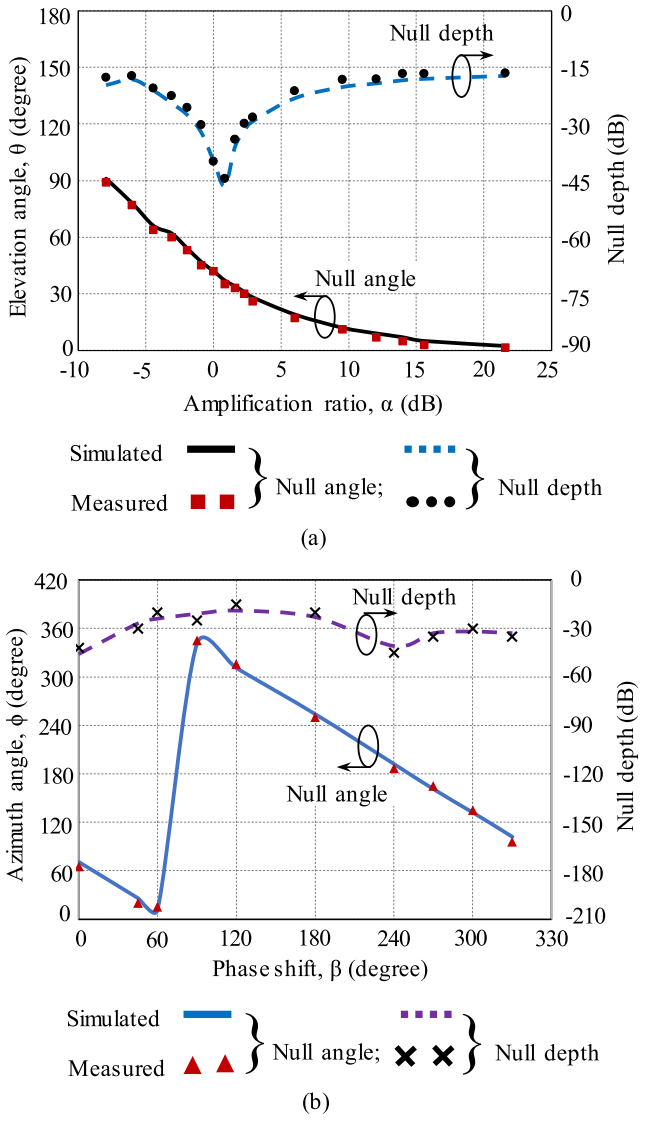

FIGURE 10. The variation of the null angle and the null depth in (a) elevation plane $\phi = 70°$ and in (b) azimuth plane $\theta = 42°$, respectively.

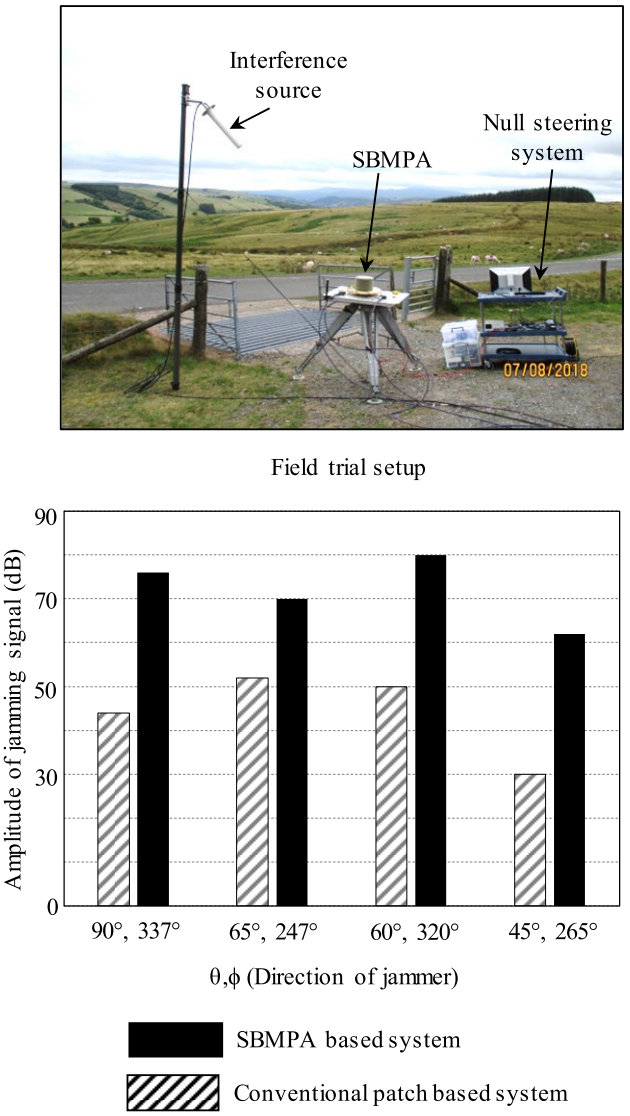

FIGURE 11. (top) Field trial set-up. (bottom) Shows SBMPA ability for sustaining relatively much higher level of jamming signal before the GNSS receiver reached the edge of collapse in comparison with a traditional patch antenna.

Fig. 8 (a)-(f) shows the radiation pattern at the elevation plane of $\phi = 70°$ while α changes from 21.5 dB to -8 dB and β remains constant at 0°. It is observed that measured results are in good agreement with the simulated results. The values α and β along with the null direction are listed in Table 2.

The direction of the null also can be steered around the azimuth plane. Fig. 9 (a)-(f) shows the null steering in the azimuth plane $\theta = 42°$. This can be achieved by changing the β while α is kept constant at 0 dB as listed in Table 2.

Fig. 10 (a) and (b) show the null depth performance for various angles in the $\phi = 70°$ elevation plane and $\theta = 42°$ azimuth plane. It is seen that the null depth is maximum between $45° < \theta < 15°$. This is because in this region both conical and axial beam have near equal amplitudes. Yet, across all elevation angles a null depth of deeper than -17 dB was observed. On the other hand, a variation of 20 dB in null depth is observed around the azimuth plane. However, across all azimuth angles the SBMPA provides a null deeper than -20 dB.

IV. LIVE ON FILED TRIALS FOR INTERFERENCE SUPPRESSION

Live on the air trials are carried out for demonstrating the interference suppression capabilities of the SBMPA. To establish the significance of the proposed system, a performance comparison is also made against a conventional patch-antenna-based system providing an axial beam. Fig. 11(top) shows the experimental setup in the field trial. A helix antenna mounted on a pole is used to provide the interference signals. The pole height is adjustable. The interference signal amplitude can be increased or decreased in steps and for this experiment a step of 2 dB at every 15 seconds is selected.

When the interference is off, the receiver was able to receive signals from 9 to 10 satellites. We gradually increased the interference and observed its level until signals from four satellites were remaining (referred to as edge of GNSS collapse). It was found that our SBMPA based system offers up to an average of 30 dB interference suppression compared to the patch-based system (Fig. 11). The significance of this 30-dB advantage is immense. It means if a patch antenna system was compromised at 1 w of power, it will take 1000 w to knock out our proposed system. Finally, an intelligent 'Scan, Monitor and Lock' algorithm is developed for realizing an autonomous null steering functionality. The algorithm runs on the Raspberry Pi and automatically steers the null in the direction of the jamming/interference. It also continuously monitors the real time satellite signals and perform a new scan when its quality falls below a threshold power level.

V. CONCLUSION

We developed a new robust form of null steering antenna for future navigation wireless systems and performed an on the air test. Compared to conventional GNSS antenna our proposed antenna offers a 30-dB jamming advantage. This means if a patch antenna-based navigation system is disturbed at 1 w of interference power, it will take 1000 w to disrupt the navigation system working on our proposed antenna system. The null steering antenna has a small size of 130 mm $\times$ 130 mm and has a small large-scale manufacturing price. Hence, it is quite suitable for imminent smart nation-based living applications.

REFERENCES

[1] M. Jones and G. Staff. (2019). Anti-Jam System: Which one Works for You?: GPS World. Gpsworld.com. [Online]. Available: https://www.gpsworld.com/anti-jam-systems-which-one-works-for-you/

[2] S. Nikolaou, R. Bairavasubramanian, C. Lugo, I. Carrasquillo, D. C. Thompson, G. E. Ponchak, J. Papapolymerou, and M. M. Tentzeris, "Pattern and frequency reconfigurable annular slot antenna using PIN diodes," *IEEE Trans. Antennas Propag.*, vol. 54, no. 2, pp. 439–448, Feb. 2006.

[3] S. Yong and J. T. Bernhard, "Reconfigurable null scanning antenna with three dimensional null steer," *IEEE Trans. Antennas Propag.*, vol. 61, no. 3, pp. 1063–1070, Mar. 2013.

[4] X. Jiang, Z. Zhang, Y. Li, and Z. Feng, "A novel null scanning antenna using even and odd modes of a shorted patch," *IEEE Trans. Antennas Propag.*, vol. 62, no. 4, pp. 1903–1909, Apr. 2014.

[5] Y. Li, Z. Zhang, C. Deng, and Z. Feng, "A simplified hemispherical 2-D angular space null steering approach for linearly polarization," *IEEE Antennas Wireless Propag. Lett.*, vol. 13, pp. 1628–1631, 2014.

[6] M. N. Solomon, "Multimode rectangular microstrip antenna for GPS applications," in *Proc. IEEE-APS Conf. Antennas Propag. Wireless Commun.*, Waltham, MA, USA, Nov. 1998, pp. 149–151.

[7] C. Deng, Y. Li, Z. Zhang, and Z. Feng, "A hemispherical 3-D null steering antenna for circular polarization," *IEEE Antennas Wireless Propag. Lett.*, vol. 14, pp. 803–806, 2015.

[8] N. R. Labadie, S. K. Sharma, and G. M. Rebeiz, "A circularly polarized multiple radiating mode microstrip antenna for satellite receive applications," *IEEE Trans. Antennas Propag.*, vol. 62, no. 7, pp. 3490–3500, Jul. 2014.

[9] B. Babakhani and S. K. Sharma, "Dual null steering and limited beam peak steering using a triple mode microstrip patch antenna," in *Proc. IEEE Int. Symp. Antennas Propag. (APSURSI)*, Fajardo, Puerto Rico, Jun. 2016, pp. 2141–2142.

[10] J. Huang, "Circularly polarized conical patterns from circular microstrip antennas," *IEEE Trans. Antennas Propag.*, vol. AP-32, no. 9, pp. 991–994, Sep. 1984.

[11] Infineon Technologies AG. Semiconductor & System Solutions. *Silicon Germanium Low Noise Amplifier for GNSS*. Accessed: Jan. 5, 2019. [Online]. Available: https://www.infineon.com/dgdl/Infineon-BGA824N6-DS-v03_00-en.pdf?fileId=db3a30433f764301013f7b53cdd02721

[12] *MAPS143, 1.4 GHz to 2.4 GHz, 4 Bit, Digital Phase Shifter*. Accessed: Jan. 11, 2019. [Online]. Available: https://cdn.macom.com/datasheets/MAPS-010143.pdf

[13] *BGA7204, 400 MHz to 2750 MHz, High Linearity Variable Gain Amplifier*. Accessed: Jan. 21, 2019. [Online]. Available: https://www.nxp.com/docs/en/data-sheet/BGA7204.pdf

[14] NovAtel. *FlexPak6 Triple-Frequency L Band GNSS Receiver*. Accessed: Jan. 23, 2019. [Online]. Available: https://www.novatel.com/products/gnss-receivers/enclosures/flexpak6/

[15] Rogers Corporation. *RT/Duroid 5880. High Frequency Laminates*. Accessed: Jan. 25, 2019. [Online]. Available: http://www.rogerscorp.com/documents/606/acs/RT-duroid-5870-5880-Data-Sheet.pdf

[16] NEMA. *National Marine Electronics Association*. Accessed: Jan. 12, 2019. [Online]. Available: https://www.nmea.org/content/STANDARDS/NMEA_0183_Standard

ARPAN PAL (Member, IEEE) received the Ph.D. degree in advanced telecommunications from Swansea University, Swansea, U.K., in 2013. From 2013 to 2014, he worked as a Research Assistant with The Institute of Electronics, Communications, and Information Technology (ECIT), Queen's University of Belfast, Belfast, U.K, on design of frequency selective surface and array antennas. From 2014 to 2019, he worked as a Research Assistant with Swansea University, on beam steering antennas, GNSS receivers, and satellite antennas. Since 2019, he has been working as a Senior Electromagnetic Modeling Engineer with Cambridge Consultants, Cambridge, U.K. His research interests involve beam-steerable antennas, phased array antennas, frequency selective surface, surface-integrated waveguide antennas, body-wearable antennas, and 5G mmwave network planning.

AMIT MEHTA (Senior Member, IEEE) received the B.Eng. degree in electronics and telecommunication from the University of Pune, India, and the M.Sc. degree in telecommunications and information networks and the Ph.D. degree in smart reconfigurable antennas from the University of Essex, U.K. He is currently the Professor & Director of the Antenna Research Group, Swansea University, U.K., where his core research interests are wireless communications, and microwave systems and antennas. He is leading large projects teams on 5G, adaptive antennas for GNSS, high throughput satellite communications, IOT, and milli-meter waves. He has successfully supervised over 20 post graduate research theses. He has over 100 technical publications. He holds three patents on the invention of the steerable beam smart antennas and concealed weapons detection systems.

ANDREW SKIPPINS received the B.Eng. degree in electronics and electrical engineering and the M.Sc. degree in communications engineering from Swansea University, U.K., in 2016 and 2017 respectively. He is currently working as a Research Assistant with the Antenna and Smart City Laboratory, Swansea University. He is a member of the Institute of Engineering and Technology.

PAUL SPICER received the B.Eng. degree in electronics and electrical engineering and the M.Sc. degree in communications engineering from Swansea University, U.K., in 2018 and 2019, respectively. He worked as a Research Assistant with the Antenna and Smart City Laboratory, Swansea University.

DARIUSH MIRSHEKAR-SYAHKAL (Fellow, IEEE) received the B.Sc. degree (Hons.) in electrical engineering from Tehran University, Tehran, Iran, in 1974, and the M.Sc. degree in microwaves and modern optics and the Ph.D. degree from University College London, University of London, U.K., in 1975 and 1979, respectively. From 1979 to 1984, he worked as a Research Fellow with University College London, on analysis and design of microwave and millimeter-wave planar transmission lines and components as well as on nondestructive evaluation of materials by electromagnetic techniques. Since 1984, he has been on the staff with the University of Essex, Colchester, U.K., where he is currently a Professor and the Head of the RF and Microwave Research Laboratory, School of Computer Science and Electronic Engineering. He owns several patents and has numerous technical publications, including a book entitled *Spectral Domain Method for Microwave Integrated Circuits* (New York: Wiley, 1990). He has been a consultant to more than ten major international companies. His current research encompasses adaptive antennas, super-compact RF filters, RF amplifier linearization, characterization and applications of liquid crystal materials at microwave and mm-wave frequencies, and numerical modeling in electromagnetics and circuits. He is a Fellow of the IET and a Chartered Engineer.